Brain Research Bulletin 243 (2026) 112016

Contents lists available at ScienceDirect

Brain Research Bulletin

journal homepage: www.elsevier.com/locate/brainresbull

Research report

Edaravone attenuates ACSL4-dependent ferroptosis in spinal motor neurons following cardiac arrest in rats

Joonseok Lee [a], Seung Hyun Lee [a], Ryunhee Kim [a], Md Shiblee Sadik Sabuj [a], Hyun-Jin Tae [a], Hoang Thi Mai [b], Su-Cheol Han [c,*], Byung-Yong Park [a,**]

[a] College of Veterinary Medicine and Institute of Animal Transplantation, Jeonbuk National University, Specialized Campus, Iksan 54596, Korea
[b] Department of Husbandry and Veterinary Medicine, School of Agriculture and Natural Resources, Vinh University, 182 Le Duan, Vinh, Nghe An, 460000, Viet Nam
[c] College of Veterinary Medicine, Jeonbuk National University, Specialized Campus, Iksan 54596, Korea

ARTICLE INFO

Keywords:
ACSL4
Cardiac arrest
Edaravone
Ferroptosis
Motor neuron
Spinal cord ischemia

ABSTRACT

The contribution of acute spinal motor neuron injury following cardiac arrest (CA) remains poorly understood. This study aimed to investigate the role of ferroptosis in CA-induced spinal cord injury and to evaluate the neuroprotective effects of edaravone. Asphyxial CA was induced in rats for 5 min, followed by resuscitation. Edaravone was administered immediately after the return of spontaneous circulation (ROSC). At 24 h post-ROSC, The CA group exhibited significant hindlimb motor deficits and reduced survival rates. Histological analysis revealed selective injury of choline acetyltransferase (ChAT)-positive motor neurons in the lumbar spinal cord, accompanied by mitochondrial shrinkage and membrane rupture, which are characteristic of ferroptosis. Immunofluorescence demonstrated a selective upregulation of the pro-ferroptotic enzyme acyl-CoA synthetase long-chain family member 4 (ACSL4) specifically in ChAT-positive motor neurons, whereas glutathione peroxidase 4 (GPX4) expression remained relatively preserved. Edaravone treatment significantly improved neurological outcomes and survival, attenuated lipid peroxidation (evidenced by decreased malondialdehyde and preserved glutathione levels), and effectively suppressed ACSL4 upregulation in the motor neurons. Furthermore, edaravone mitigated neuroinflammation by reducing astrogliosis and microglial activation. These findings provide the first evidence that ACSL4-mediated ferroptosis is a key driver of acute spinal motor neuron injury following CA. Edaravone exerts potent neuroprotection by targeting this pathway, suggesting its therapeutic potential for ameliorating spinal cord injury in patients with CA.

1. Introduction

Post-cardiac arrest syndrome (PCAS), which patients often experience following cardiac arrest (CA), is characterized by systemic ischemia-reperfusion injury (IRI) (Neumar et al., 2008). PCAS may also manifest as ischemic spinal cord injury, followed by motor dysfunction and paraplegia, with reported selective vulnerability in the lumbosacral region (Cheshire et al., 1996; Duggal and Lach, 2002). Despite this, the spinal cord remains a relatively underexplored target in the context of post-CA injury, and the underlying mechanisms driving spinal motor neuron damage and therapeutic approaches against it have not been fully elucidated (Kudo et al., 2006; Wang et al., 2023).

Several studies have reported motor neuron degeneration in the lumbar spinal cord following CA (Ahn et al., 2023; Duggal and Lach, 2002; Keilhoff et al., 2021; Lee et al., 2021). However, the mechanisms underlying acute-phase spinal motor neuron injury remain poorly understood (Ahn et al., 2020). Recent studies have identified ferroptosis, a regulated form of cell death driven by iron-dependent lipid peroxidation, as a key contributor to central nervous system (CNS) ischemic injury, including stroke and spinal cord ischemia-reperfusion injury (SCIRI) (Alim et al., 2019; Cui et al., 2021; Dong et al., 2023; Tuo et al., 2022). This non-apoptotic programmed cell death is strongly associated

* Correspondence to: College of Veterinary Medicine, Jeonbuk National University, Specialized Campus, Gobong-ro 79, Iksan 54596, Jellabuk-do, Republic of Korea.
** Correspondence to: College of Veterinary Medicine and Institute of Animal Transplantation, Jeonbuk National University, Specialized Campus, Gobong-ro 79, Iksan 54596, Jellabuk-do, Republic of Korea.
E-mail addresses: haseul@jbnu.ac.kr (J. Lee), seung999@jbnu.ac.kr (S.H. Lee), ryunhee15@jbnu.ac.kr (R. Kim), shiblee@jbnu.ac.kr (M.S.S. Sabuj), hjtae@jbnu.ac.kr (H.-J. Tae), maiht@vinhuni.edu.vn (H. Thi Mai), vethansc@jbnu.ac.kr (S.-C. Han), parkb@jbnu.ac.kr (B.-Y. Park).

https://doi.org/10.1016/j.brainresbull.2026.112016
Received 19 January 2026; Received in revised form 12 June 2026; Accepted 22 June 2026
Available online 24 June 2026

with excessive reactive oxygen species (ROS) production after IRI (Chen et al., 2021; Dixon et al., 2012). However, most findings have been derived from focal ischemia models, and the role of ferroptosis in the unique systemic ischemia-reperfusion pathology of CA remains unclear.

Among the molecular regulators of ferroptosis, acyl-CoA synthetase long-chain family member 4 (ACSL4) has emerged as a key pro-ferroptotic enzyme that promotes lipid peroxidation by enriching polyunsaturated fatty acids in cellular membranes, thereby increasing susceptibility to ferroptotic cell death (Doll et al., 2017; Yuan et al., 2016). Although ACSL4-mediated ferroptosis has been implicated in neuronal injury in several CNS ischemia models (Cui et al., 2021; Tuo et al., 2022), it remains unknown whether this pathway contributes to spinal motor neuron injury following CA.

Edaravone is an FDA-approved reactive oxygen species (ROS) scavenger that has demonstrated protective effects against various central nervous system (CNS) disorders, including stroke and Amyotrophic Lateral Sclerosis (ALS) (Kubo et al., 2009; Rothstein, 2017). Through its potent ROS-scavenging capability, edaravone mitigates excessive oxidative stress generated during ischemia-reperfusion. Consistent with this, its neuroprotective efficacy in SCIRI has been well documented (Suzuki et al., 2005). Recently, the anti-ferroptotic effects of edaravone have been investigated in the context of stroke (Liu et al., 2022; Xiao et al., 2024) and traumatic spinal cord injury (Pang et al., 2022). However, its therapeutic potential in spinal cord injury after CA remains unknown.

Therefore, in this study, we aimed to elucidate the role of ACSL4-mediated ferroptosis in acute spinal motor neuron injury following asphyxial cardiac arrest and evaluate whether edaravone exerts neuroprotective effects by targeting this specific pathway.

2. Materials and methods

2.1. Experimental animals

Male Sprague-Dawley (SD) rats (n = 69; 300 ± 30 g) were supplied by Hannil Experimental Animal Center (Wanju, South Korea). They were housed under standard conditions, maintaining adequate control of temperature (23 ± 2°C) and humidity (60 ± 10%) with a 12 h light/12 h dark day cycle. The animals had ad libitum access to food and water. All experimental protocols were approved based on ethical procedures and scientific care by the Jeonbuk National University Institutional Animal Care and Use Committee (approval no. NON2025–008). The rats were randomly divided into three groups: sham (n = 15), CA (n = 37), and CA + Edaravone (CA+Eda; n = 17). Animals were sacrificed 24 h after CA/ROSC, the time point when ferroptosis markers are most prominently expressed in SCIRI, based on a previous study (Dong et al., 2023).

2.2. Induction of asphyxial cardiac arrest and drug administration

CA and cardiopulmonary resuscitation (CPR) were performed using previously published procedures with minor modifications (Ahn et al., 2020). Briefly, the rats were anesthetized with 4–5% isoflurane before endotracheal intubation. After intubation, the rats were anesthetized with 2–3% isoflurane and mechanically ventilated using a rodent ventilator (Harvard Apparatus, Hollison, MA, USA) to maintain their breathing during CPR. To monitor peripheral oxygen saturation (SpO_2), a pulse oximetry oxygen saturation probe (Nonin Medical Inc., Plymouth, MN, USA) was attached to the left foot. To assess the electrocardiograms (ECG), electrocardiographic probes (GE Healthcare, Milwaukee, WI, USA) were attached to the right arm, right leg, and left leg. Catheters for the mean arterial pressure (MAP) probe (MLT 1050 1050/D; AD Instruments, Bella Vista, Austria) and intravenous injections were inserted into the right femoral artery and left femoral vein, respectively. To induce asphyxia cardiac arrest, vecuronium bromide (Vecarone Inj., Reyon Pharmaceutical Co., Ltd., Jincheon, South Korea) was injected intravenously, anesthesia was ceased, and mechanical ventilation was withdrawn from the rats. CA was determined based on a MAP of < 25 mmHg and subsequent pulseless electric activity (PEA). CA was confirmed 3–4 min after vecuronium bromide injection. Five minutes after CA confirmation, sodium bicarbonate (Sodium Bicarbonate Inj. 8.4%, Daihan Pharm. Co., Ltd., Seoul, South Korea) and epinephrine (Daihan Pharm. Co., Ltd., Seoul, South Korea) were injected intravenously, and mechanical ventilation with 100% oxygen and manual chest compression (300 times/min) was administered until the MAP reached 60 mmHg, ECG activity was observed, and return of spontaneous circulation (ROSC) was confirmed. Immediately after ROSC, the CA + Edaravone group received edaravone (3 ml/kg) (Radicut Inj., Mitsubishi Tanabe Pharma, Osaka, Japan) (Kubo et al., 2009). Edaravone was intravenously administered at a rate of 1 ml/min through a catheter inserted into the left femoral vein. After the animal regained spontaneous breathing and hemodynamic stability, the catheters and intubation were removed, and the animal was extubated. All procedures were performed under normothermic conditions (Fig. 1A). Animals that failed to recover spontaneous respiration within 1 h were excluded from the study.

2.3. Evaluation of hindlimb motor function

Hindlimb motor function was evaluated 24 h after CA/ROSC based on the Tarlov scoring system by two investigators blinded to group identity: 0, spastic paraplegia and no voluntary movement of the lower limbs; 1, spastic paraplegia and weak hind limb motor function of the lower limbs; 2, good antigravity strength with some lower limb movement but inability to stand; 3, abnormal standing but unable to walk normally; and 4, normal motor function (Ahn et al., 2023).

2.4. Tissue preparation for histological analysis

All animals were deeply anesthetized with urethane (1.5 g/kg) (Daejung Chemicals & Metals Co., Ltd., Siheung, South Korea) and perfused intracardially with 0.1 M PBS (pH 7.4), followed by fixation with 4% paraformaldehyde (PFA) in 0.1 M PBS. The lumbar spinal cord L2–L6 segments were identified based on the anatomical morphology of the rat spinal cord (Fig. 1G). Lumbar enlargement of the spinal cord in rats is located at the vertebral T12-L1 level, corresponding to the spinal cord segments L1-L5. We harvested a 2 cm spinal cord segment in the caudal direction from the lower border of the T1 vertebra (Wang et al., 2020). The spinal cord was removed, post-fixed overnight in PFA, and cryoprotected for 24 h in 30% sucrose solution. The spinal cord tissues were embedded in OCT blocks. Serial 30 μm thick coronal sections were obtained using a cryostat and stored at 4°C.

2.5. Hematoxylin and eosin (H&E) staining

H&E staining was used to evaluate morphological changes in spinal cord motor neurons after CA/ROSC. Spinal cord sections were mounted on slides and stained using an H&E Stain Kit (ScyTek Laboratories, Logan, UT, USA) according to the manufacturer's instructions. Briefly, the sections were stained with hematoxylin and eosin, rinsed, dehydrated through graded ethanol, cleared in xylene, and coverslipped with mounting medium. Images of the sections were obtained and evaluated at a magnification of 200 × under a light microscope (Axio Imager A1; Carl Zeiss, Oberkochen, Germany) by two investigators blinded to the study design.

2.6. Transmission electron microscopy (TEM)

Transmission Electron Microscopy was performed to observe the ultrastructure of the mitochondria in the rat spinal cord. Spinal cords were collected and fixed in 2.5% glutaraldehyde for overnight at 4 °C. All samples were then transferred to 1% osmium tetroxide for 1.5 h at 4

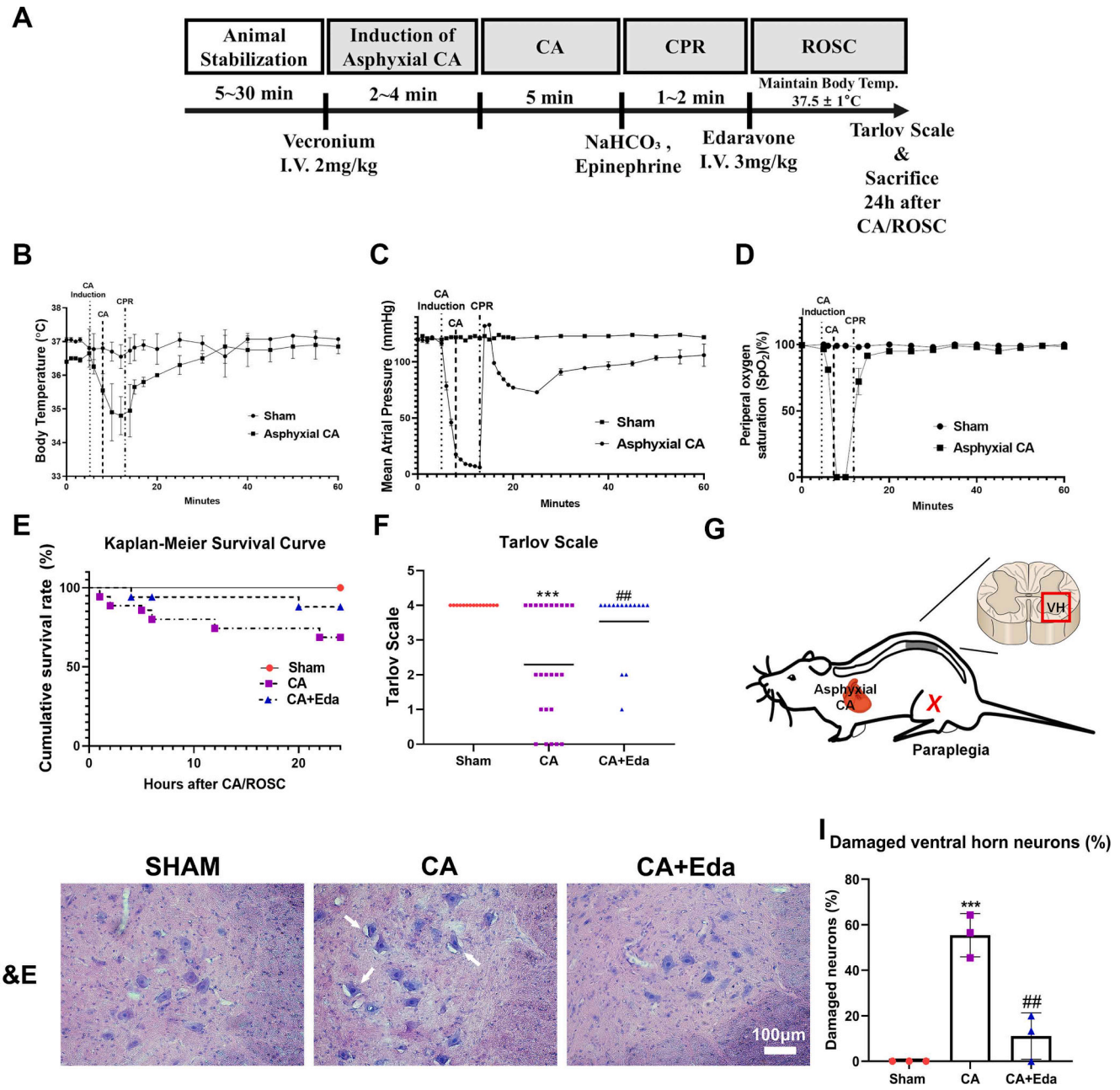

Fig. 1. Edaravone improves survival, neurological outcomes, and spinal motor neuron morphology after cardiac arrest. (A) Schematic representation of the experimental timeline and design. CA induction, CPR, and ROSC were performed at designated times. Edaravone was administered immediately after ROSC. Hindlimb motor function assessment and sacrifice for analyses of the lumbar spinal cord were conducted 24 h after CA/ROSC. (B-C) Physiological variables and temperature flow after CA/CPR. (B) Body temperature. (C) Mean atrial pressure (MAP) (D) and peripheral oxygen saturation (SpO_2) of representative animals are shown during CA induction, CA, and CPR. Data are presented as mean ± SD (E) Kaplan–Meier survival curves showing the cumulative survival of rats in each group (sham, n = 15; CA, n = 37; CA+Eda, n = 17) during the 24-h period after CA/ROSC. Survival was significantly improved in the CA + Eda group compared with the CA group (log-rank test, $p = 0.0279$). (F) Hindlimb motor function assessed based on the Tarlov scale. The Tarlov scale was graded as follows: 0, complete paraplegia; 1, noticeable movement at joints; 2, good joint movement without the ability to stand; 3, ability to stand but inability to walk normally; and 4, normal motor function. Data are presented as mean ± standard deviation (SD). Statistical analysis was performed using Kruskal – Wallis test followed by Tukey's post hoc test (Sham, n = 15; CA, n = 24; CA+Eda, n = 15). * $p < 0.05$, ** $p < 0.01$, *** $p < 0.001$ vs. Sham group; #$p < 0.05$, ##$p < 0.01$ vs. CA group. (G) Histological evaluation of the ventral horn of the lumbar spinal cord was conducted. (H) Edaravone alleviates neuronal cell shrinkage in the lumbar spinal cord 24 h after CA/ROSC. Representative H&E-stained image of the ventral horn of the lumbar spinal cord. In the CA group, neuronal cell shrinkage (arrowheads) were observed in the ventral horn of the spinal cord. Scale bar, 100μm. Magnification, × 200. (I) Quantitative analysis of damaged cell per 400 × 400 μm in each group. Statistical analysis was performed using one-way ANOVA followed by Tukey's post hoc test ($n = 3$). *** $p < 0.001$ vs. Sham, ### $p < 0.001$ vs. CA group.

°C. The samples were dehydrated, embedded in epoxy resin, and sliced using an ultramicrotome (Powertome XL; Boeckeler Instruments Inc., Tucson, AZ, USA). Ultrathin sections (60–80 nm) were mounted on copper grids and examined using a Bio-transmission electron microscope (Talos L120C G2; Thermo Fisher Scientific, Waltham, MA, USA).

2.7. GSH, MDA, total iron ion assay

Total glutathione (GSH) levels in the spinal cord tissue were quantified using a commercial glutathione assay kit (EZ-Glutathione Assay Kit, DG-GLU200; Dogenbio, Seoul, South Korea). Malondialdehyde

(MDA) levels, an index of lipid peroxidation, were determined using a TBARS assay kit (Cayman Chemical, Ann Arbor, MI, USA). Total iron ion levels were measured using a colorimetric iron assay kit (Abcam, ab83366; Cambridge, UK) according to the manufacturer's instructions.

2.8. In vivo western blot analysis

Spinal cord tissues of L2–L6 segments were harvested with PBS perfusion and homogenized on ice in a mixture of tissue protein extraction reagent (T-PER), 10 × phosphatase inhibitors (PhosSTOP™, Roche, Basel, Switzerland), and 25 × protease inhibitor cocktail (cOmplete™, Roche, Basel, Switzerland). The total protein concentration in the spinal cord was measured using a bicinchoninic acid (BCA) protein assay (Pierce™ BCA Protein Assay Kit, Thermo Scientific, Waltham, MA, USA). Forty-five μg of the protein were separated using 12% sodium dodecyl sulfate-polyacrylamide gel electrophoresis (SDS-PAGE) and transferred onto a polyvinylidene fluoride (PVDF) membrane, which was blocked with 5% bovine serum albumin at room temperature for 1 h followed by overnight incubation with primary antibodies against glutathione peroxidase 4(GPX4, 1:500; ab125066, Abcam, Cambridge, UK), acyl-CoA synthetase long-chain family member (ACSL4, 1:5000; ab169755, Abcam, Cambridge, UK) and cyclooxygenase−2 (COX2, 1:1000; #12282, Cell Signaling Technology, Danvers, MA, USA) at 4°C. After rinsing with Tris-buffered saline with Tween 20 (TBST), the membrane was incubated with secondary antibody (anti rabbit IgG, HRP-linked Antibody, 1:1000, Invitrogen, Waltham, MA, USA) at room temperature for 1 h and visualized with chemiluminescence using a chemiluminescent imaging system (Amersham™ ImageQuant™ 500, CYTIVA, Marlborough, MA, USA), and β-actin was used as a reference protein.

For quantitative analysis of protein levels, densitometry analysis was conducted using ImageJ software (National Institute of Health, Bethesda, MD, USA).

2.9. Immunofluorescence (IF) double staining

IF double staining was conducted to identify the expression of ferroptosis-related proteins in neurons (NeuN-positive cells) and motor neurons (ChAT-positive cells). The frozen sections were washed with phosphate-buffered saline (PBS) and blocked with serum-free protein block (X0909, DAKO, USA) at room temperature for 1 h. The Sections were incubated with the primary antibodies: rabbit anti-Acyl-CoA synthetase long-chain family member (ACSL4, 1:100, ab169755, Abcam, Cambridge, UK), mouse anti-Choline Acetyltransferase (ChAT, 1:100, MA5–31382, Invitrogen, Waltham, MA, USA)and mouse anti-NeuN (NeuN, 1:100, MAB377, Millipore, Burlington, MA, USA) antibodies for 2 days at 4℃, washed in phosphate-buffered saline with 0.3% Triton X−100 (PBST), and incubated with secondary antibodies (Goat Anti-Mouse IgG H+L Cross-Absorbed secondary antibody Alexa fluor 594, 1:500, A−11005, Invitrogen, Waltham, MA, USA; Goat Anti rabbit IgG H&L Alexa 488, 1:500, ab150077, Abcam, Cambridge, UK)) for 1 h at room temperature. Immunofluorescence images were obtained using a confocal microscope (LSM 980; Carl Zeiss, Oberkochen, Germany). The intensity was quantified using ImageJ software (National Institutes of Health, Bethesda, MD, USA). The average mean intensity values are expressed as the mean ± SD. Since motor neurons are located in the ventral horn of the lumbar spinal cord gray matter, images were acquired at a resolution of 400 × 400 μm in the center of the ventral horn (Fig. 1B).

2.10. Immunohistochemistry (IHC) staining

IHC was performed to evaluate the immunoreactivity of ionized calcium-binding adapter molecule−1 (Iba−1) and glial fibrillary acidic protein (GFAP), according to a previously published method (Ahn et al., 2023), with modifications. Briefly, spinal cord sections were quenched by immersion in 0.3% hydrogen peroxide(H_2O_2) for 20 min and then in 5% normal goat serum for 1 h. After blocking, the sections were incubated overnight with rabbit anti-ionized calcium-binding adapter molecule−1 (Iba−1, 1:250; Genetex, Irvine, CA, USA) as a microglia marker and rabbit anti-glial fibrillary acidic protein (GFAP, 1:250; Genetex, Irvine, CA, USA), an astrocyte marker. After washing, the sections were incubated with biotinylated goat anti-rabbit IgG (1:200; BA−5000, Vector, Newark, California, USA) for 2 h, followed by incubation with a streptavidin peroxidase complex for 1 h. The sections were visualized using 0.2% 3, 3'-diaminobenzidine solution. Images were obtained at a magnification of 200 × under a light microscope (Axio Imager A1; Carl Zeiss, Oberkochen, Germany), and quantitative analysis of Iba−1 and GFAP immunoreactivity as relative optical density (ROD) was performed using ImageJ software.

2.11. SH-SY5Y cell culture

SH-SY5Y cells (Korean Cell Line Bank, Seoul, South Korea) were cultured in DMEM (Gibco, Carlsbad, CA, USA) enriched with 10% FBS and antibiotics. Incubation was conducted at 37 °C under 5% CO_2 using an SMA−30D incubator (ASTEC Co., Ltd., Fukuoka, Japan). To control the confluency and sustain viable proliferation, the cells were dissociated every 72 h with 0.05% trypsin and 0.02% EDTA (WELGENE Inc., Gyeongsan, South Korea).

2.12. Cell viability and cytotoxicity assay

Cell viability and cytotoxicity were assessed using MTT (Sigma-Aldrich, St. Louis, MO, USA). SH-SY5Y cells were pretreated with 1 μM Ferrostatin−1 (Sigma-Aldrich, St. Louis, MO, USA) and 200 μM edaravone for 1 h. To assess cell viability, the cells were co-incubated with 400 μM H_2O_2 (Fujifilm Wako, Osaka, Japan) for 24 h. Following treatment with 0.05 mg/ml MTT, cells were incubated for 3 h. Formazan crystals were solubilized in DMSO, and absorbance was measured at 570 nm using a Versa Max microplate reader (Molecular Devices, San Jose, CA, USA).

2.13. In vitro western blot analysis

SH-SY5Y cells were pretreated with 1 μM Ferrostatin−1 or 200 μM edaravone for 1 h and then exposed to 400 μM H_2O_2 for 24 h before protein extraction. Harvested cells were lysed on ice in radioimmunoprecipitation assay (RIPA) buffer (Biosesang, Yongin, South Korea) supplemented with the same phosphatase and protease inhibitors used for the in vivo samples. Western blotting was then performed as described above using antibodies against ACSL4 and β-actin.

2.14. Statistical analysis

Statistical analyses were performed using GraphPad Prism v. 8.0 (GraphPad Software, La Jolla, CA, USA). Data are expressed as mean ± standard deviation (SD), and *p-values* < 0.05 were considered statistically significant. Comparisons between groups were performed using one-way ANOVA, followed by Tukey's post hoc test. For comparisons involving two independent variables (cell type and treatment group), a two-way ANOVA with repeated measures followed by Sidak's post hoc test was utilized. Post hoc power analyses for fluorescence-based histological quantification were performed using G*Power with animal-level means as the independent statistical units.

3. Results

3.1. Edaravone improves survival and motor function and attenuates early motor neuronal injury in the lumbar spinal cord after cardiac arrest

To confirm the proper induction of CA and evaluate the systemic

physiological response following CA, the core body temperature, MAP, and SpO_2 were monitored (Fig. 1B-D). No significant differences were observed in these parameters between the sham and CA groups after CA induction, indicating that CA was induced under comparable physiological conditions in both groups. The cumulative survival rate was assessed using Kaplan–Meier survival analysis ($p = 0.0279$), and edaravone treatment significantly improved survival following CA (Fig. 1E). Hindlimb motor function assessed using the Tarlov scale revealed significant motor deficits in rats subjected to CA (mean score = 2.29), whereas edaravone-treated rats showed significantly improved motor function (mean score = 3.53, $p < 0.05$) (Fig. 1F).

Histological evaluation of the lumbar spinal cord using H&E staining was conducted in the L2-L6 spinal cord (Fig. 1G). White arrowheads indicate shrinkage of neuronal cell bodies and increased pericellular space in the ventral horn following CA (Fig. 1H). These ischemia-reperfusion-induced morphological changes were largely attenuated in the CA + Eda group, indicating the neuroprotective effect of edaravone on spinal motor neurons after CA (Fig. 1I). ChAT immunofluorescence staining was performed to further evaluate motor neuron changes after CA/ROSC (Supplementary fig. 4A-C). Quantitative analysis revealed no significant difference in the number of ChAT-positive motor neurons among the Sham, CA, and CA + Eda groups (Supplementary fig. 4B). However, ChAT-positive motor neurons in the CA group exhibited morphological abnormalities, including soma shrinkage and enlargement of the pericellular space, whereas these changes were less prominent in the CA + Eda group (Supplementary fig. 4 C). These findings suggest that the 24 h time point reflects early morphological injury of spinal motor neurons rather than overt motor neuron loss.

3.2. Edaravone mitigates ferroptosis-related molecular and ultrastructural changes in the lumbar spinal cord

To investigate ferroptosis-related alterations induced by CA and their modulation by edaravone in the lumbar spinal cord, MDA, GSH, and total iron levels were measured, and TEM was performed (Fig. 2A-E). CA significantly increased MDA and total iron levels, whereas these increases were attenuated in the CA + Eda group (Fig. 2C, D). In contrast, GSH levels were significantly reduced in the CA group and preserved by edaravone treatment, suggesting the maintenance of antioxidant capacity (Fig. 2E). Ultrastructural changes observed by TEM revealed characteristic features consistent with ferroptosis in the CA group, including mitochondrial shrinkage, dilated internal cristae, and increased membrane density (black arrowheads). These abnormalities were alleviated in the edaravone-treated group, indicating preservation of mitochondrial integrity (Fig. 2A, B). In parallel, CA altered the expression of ferroptosis-related proteins. Western blot analysis showed that GPX4, a central ferroptosis suppressor, was significantly decreased in the CA group compared to the sham group, whereas ACSL4, a key pro-ferroptotic promoter, was markedly increased after CA. Edaravone treatment restored GPX4 expression to near-sham levels and significantly suppressed ACSL4 upregulation (Fig. 2F).

3.3. Edaravone down regulates ACSL4 in lumbar spinal motor neurons

To determine the cellular specificity of ACSL4 upregulation following CA, ACSL4 expression was quantified in ChAT-positive spinal motor neurons and compared with the NeuN-positive general neuronal population using double immunofluorescence staining, with analyses focused on the ventral horn of the L2–L6 spinal segments (Fig. 3E).

Quantitative analysis of the mean fluorescence intensity showed that ACSL4 expression was significantly increased in ChAT-positive motor neurons in the CA group compared that to in the sham group. This increase was attenuated by edaravone treatment (Fig. 3A, B and F). In NeuN-positive neurons, ACSL4 fluorescence intensity was also elevated following CA and reduced by edaravone treatment (Fig. 3C, D and G).

To further investigate whether ACSL4 is predominantly upregulated in motor neurons, we quantified the proportion of ACSL4-positive cells within ChAT-positive and NeuN-positive populations. In the CA group, the percentage of ACSL4-positive cells was significantly higher in ChAT-positive motor neurons (86.5 ± 6.3%) compared to the general NeuN-positive neuronal population (53.2 ± 7.9%; ***$P < 0.001$). Notably, such a significant discrepancy between the two cell types was not observed in the Sham or CA + Eda groups (Fig. 3H).

Together, these results demonstrate that ACSL4 upregulation following CA is predominantly concentrated in ChAT-positive motor neurons, indicating the selective vulnerability of spinal motor neurons to ACSL4-associated ferroptotic stress. Post hoc power analyses were performed for the fluorescence-based histological quantifications shown in Figs. 3F and 3G, and the results are summarized in Supplementary Table 1.

3.4. GPX4 expression in spinal motor neurons remains unaltered following cardiac arrest

Notably, despite the changes in GPX4 expression observed at the tissue level in the lumbar spinal cord, immunofluorescence analysis revealed no significant differences in GPX4 expression among the groups in ChAT-positive motor neurons (Fig. 4A-C). Post hoc power analyses were performed for the fluorescence-based histological quantifications shown in Fig. 4C, and the results are summarized in Supplementary Table 1.

3.5. Edaravone reduces neuroinflammation in the lumbar spinal cord

To investigate the neuroinflammatory response following CA, immunohistochemistry was performed for Iba−1 and GFAP, markers of activated microglia and astrocytes, respectively. In the CA group, marked increases in Iba−1 and GFAP immunoreactivity were observed in the ventral horn of the lumbar spinal cord, indicating robust microglial activation and reactive astrogliosis. Quantitative analysis of relative optical density (ROD) revealed that both Iba−1 and GFAP immunoreactivity were significantly elevated in the CA group compared to that in the sham group. Edaravone treatment significantly attenuated these increases, demonstrating the suppression of glial activation (Fig. 5A–D). Western blot analysis further revealed a significant upregulation of COX−2, a pro-inflammatory mediator, in the lumbar spinal cord following CA. This increase was markedly reduced in the CA + Eda group (Fig. 5E). Together, these results indicate that edaravone attenuates CA-induced neuroinflammatory responses in the lumbar spinal cord, contributing to its overall neuroprotective effect in spinal cord ischemia–reperfusion injury.

3.6. Edaravone attenuated H_2O_2-induced cytotoxicity and ACSL4 upregulation in SH-SY5Y cells

To examine whether ACSL4 upregulation is associated with oxidative stress-induced neuronal injury and whether this response is attenuated by edaravone or by ferroptosis inhibition, SH-SY5Y cells were exposed to H_2O_2 with or without pretreatment with edaravone or the ferroptosis inhibitor ferrostatin−1 (Supplementary fig. 5 A, B)·H_2O_2 exposure significantly reduced cell viability and increased ACSL4 expression compared with the control group. In contrast, pretreatment with edaravone or ferrostatin−1 attenuated the H2O2-induced reduction in cell viability and suppressed ACSL4 upregulation. These findings suggest that oxidative stress-induced neuronal injury is accompanied by ACSL4 upregulation and that both edaravone and ferroptosis inhibition attenuate this response.

4. Discussion

In this study, edaravone improved both survival rates and hindlimb motor function 24 h after 5 min CA/ROSC and preserved spinal motor

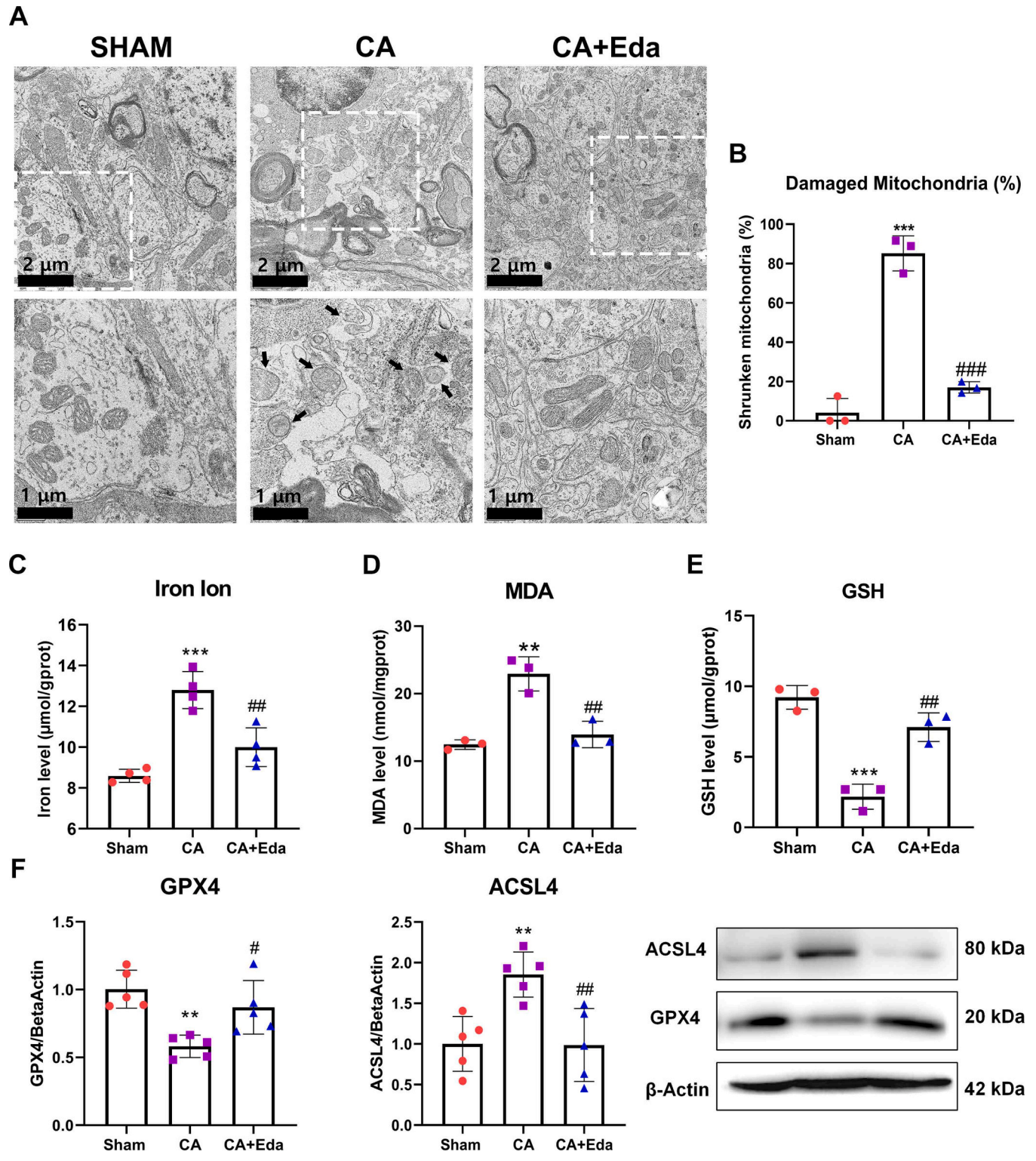

Fig. 2. Edaravone attenuates ferroptosis-related factors and ultrastructural alterations in the lumbar spinal cord after cardiac arrest. (A) Representative TEM images of the ventral horn of the lumbar spinal cord. The upper panels show images acquired at × 5000 magnification, and the lower panels show higher-magnification images at × 10,000. Black arrows indicate abnormal mitochondria. (B) Quantitative analysis of the damaged mitochondria per 4 × 4μm. *** $p < 0.001$ vs. Sham, ### $p < 0.001$ vs. CA group.(C–E) Quantitative analysis of total iron ion content ($n = 4$) (C), malondialdehyde (MDA) levels (n = 3) (D), and total glutathione (GSH) levels ($n = 3$) (E) in the lumbar spinal cord 24 h after CA/ROSC. Cardiac arrest significantly increased iron ion accumulation and lipid peroxidation, accompanied by depletion of GSH, whereas edaravone treatment significantly attenuated these changes. (F) Western blot analysis and densitometric quantification of ferroptosis-related proteins GPX4 ($n = 5$) and ACSL4 ($n = 5$) in the lumbar spinal cord. GPX4 expression was significantly decreased, whereas ACSL4 expression was markedly increased in the CA group compared to the sham group. These alterations were significantly reversed by edaravone treatment. Representative immunoblots are shown on the right, with β-actin as the loading control. Data are presented as mean ± SD. Statistical analyses were performed using one-way ANOVA followed by Tukey's post hoc test. *$p < 0.05$, **$p < 0.01$, ***$p < 0.001$ vs. sham group; # $p < 0.05$, ## $p < 0.01$ vs. CA group.

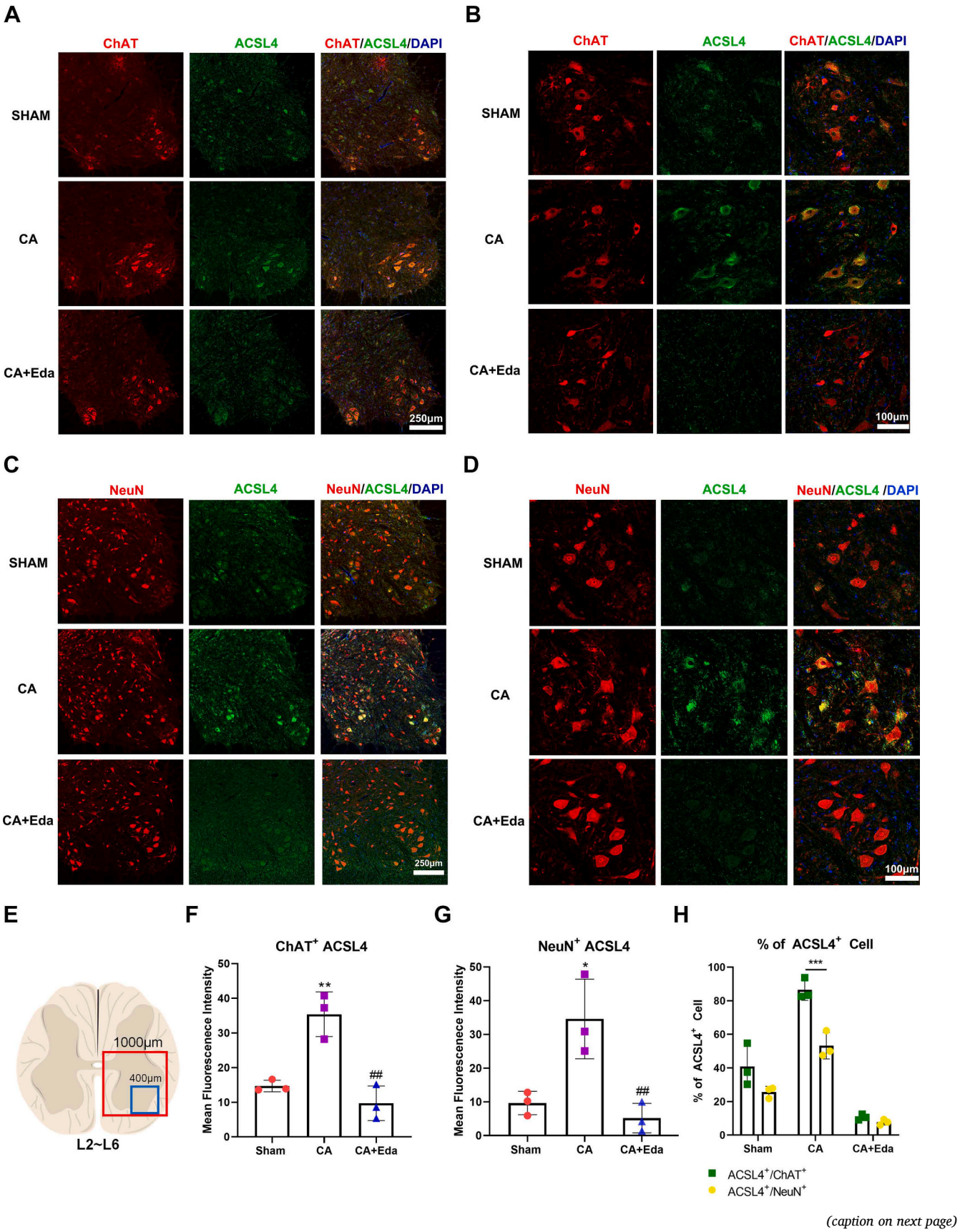

(caption on next page)

Fig. 3. Selective upregulation of ACSL4 in ChAT-positive spinal motor neurons following cardiac arrest and its suppression by edaravone (A–D) Representative double immunofluorescence images showing ACSL4 expression (green) in ChAT-positive spinal motor neurons (A, B; red) and NeuN-positive neurons (C, D; red) in the ventral horn of the lumbar spinal cord (L2–L6). The nuclei were counterstained with DAPI (blue). Images in (A, C) were acquired at low magnification (field size: 1000 ×1000μm), and images in (B, D) were acquired at high magnification (field size: 400 ×400μm). (E) Schematic illustration indicating the anatomical location of the lumbar spinal cord (L2–L6) and ventral horn region used for image acquisition, with magnification levels indicated. (F, G) Quantification of the mean fluorescence intensity of ACSL4 in ChAT-positive motor neurons (F) and NeuN-positive neurons (G). ACSL4 expression was significantly increased after CA and attenuated by edaravone treatment. Each dot represents one animal; three ROIs from one anatomically matched high-magnification image were averaged per animal. Statistical analysis was performed using one-way analysis of variance (ANOVA) followed by Tukey's post-hoc test. n = 3, respectively, $*p < 0.05$, $**p < 0.01$, $***p < 0.001$ vs. sham group; $\# p < 0.05$, $\#\# p < 0.01$ vs. CA group. (H) Quantification of the proportion of ACSL4-positive cells within NeuN-positive neurons and ChAT-positive motor neurons. Statistical analysis was performed using two-way ANOVA with repeated measures, followed by Sidak's post hoc test. n = 3, respectively. *** $p < 0.001$ indicates a significant difference between ChAT-positive motor neurons and NeuN-positive neurons within the same treatment group. Data are presented as mean ± SD. Scale bars: 250 μm in (A, C); 100 μm in (B, D).

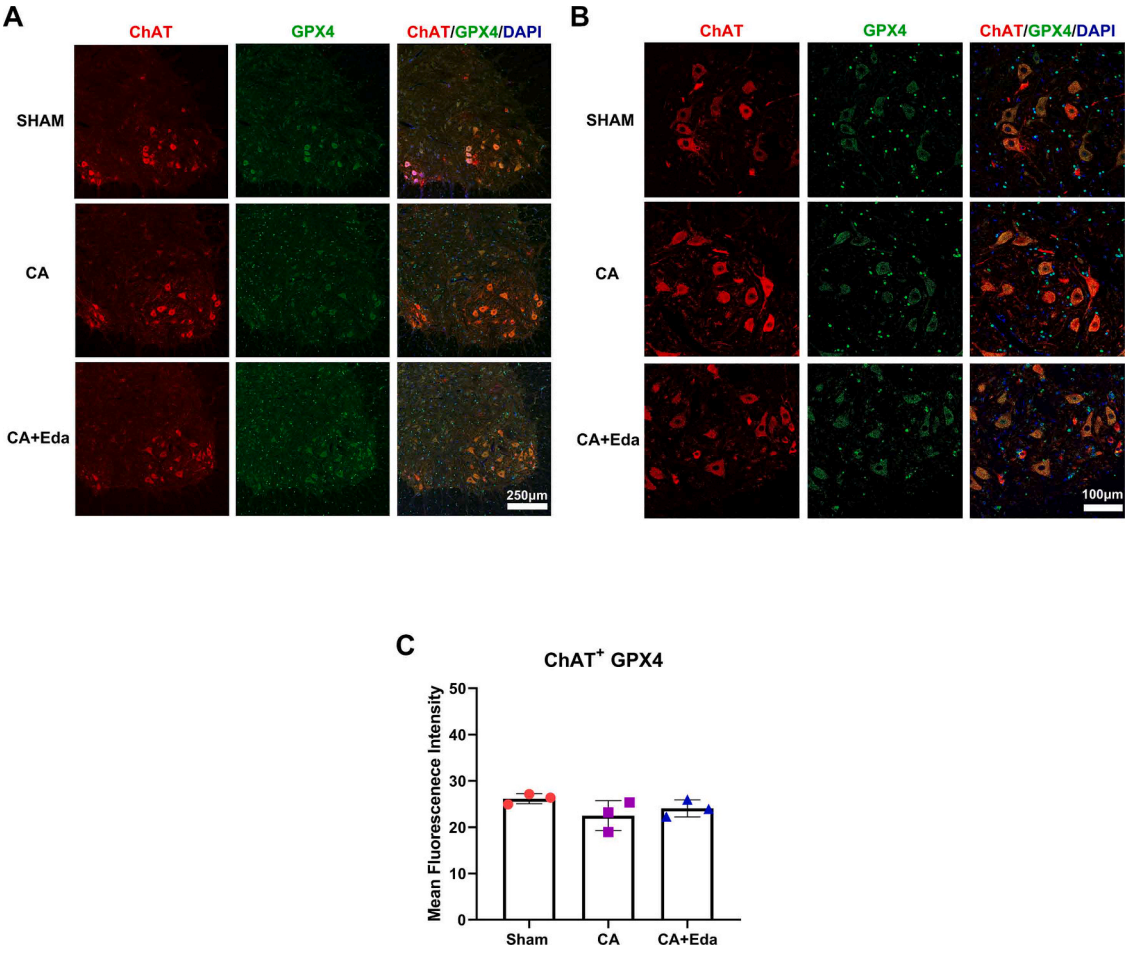

Fig. 4. GPX4 expression in spinal motor neurons remains unaltered following cardiac arrest (A, B) Representative double immunofluorescence images showing GPX4 expression (green) in ChAT-positive spinal motor neurons (red) in the ventral horn of the lumbar spinal cord (L2–L6) across the Sham, CA, and CA + Eda groups. The nuclei were counterstained with DAPI (blue). Images in (A) were acquired at low magnification (field size: 1000 ×1000 μm), and images in (B) were acquired at high magnification (field size 400 ×400 μm). (C) Quantification of GPX4 mean fluorescence intensity in ChAT-positive motor neurons. No significant differences in GPX4 expression were observed among the Sham, CA, and CA + Eda groups. Each dot represents one animal; three ROIs from one anatomically matched high-magnification image were averaged per animal. Data are presented as mean ± SD. Statistical analysis was performed using one-way ANOVA followed by Tukey's post hoc test. n = 3, respectively. Scale bars: 250 μm in (A); 100 μm in (B).

neuron morphology. Neuroinflammation, mediated by astrogliosis and microglial activation, was attenuated by edaravone treatment in a cardiac arrest model. Neuroinflammation is a common pathological response to CNS ischemic injury (Crack and Wong, 2008). Previous studies have reported improved survival following edaravone treatment in various cardiac arrest models, including rat models of ventricular fibrillation (Kubo et al., 2009; Qin et al., 2016). Moreover, the protective effects of edaravone on spinal neurons have been demonstrated in spinal cord injury models, including contusive and ischemic types (Dong et al., 2023; Ishii et al., 2018; Özgiray et al., 2012; Suzuki et al., 2005). These studies collectively support the neuroprotective role of edaravone in spinal cord ischemic reperfusion injury (IRI).

Hindlimb motor deficits after spinal cord IRI are attributed to the degeneration of motor neurons in the lumbar spinal region (Sakurai et al., 1998). Previous studies across various species, including rats, rabbits, and mice, have consistently reported motor neuron degeneration and apoptosis in the lumbar gray matter following 11–15 min of spinal cord ischemia (Kanellopoulos et al., 1997; Sakurai et al., 1998; Lang-Lazdunski et al., 2000). In a rat asphyxial CA model, ChAT-positive motor neuron damage was detectable at 24 h (Ahn et al., 2020), and

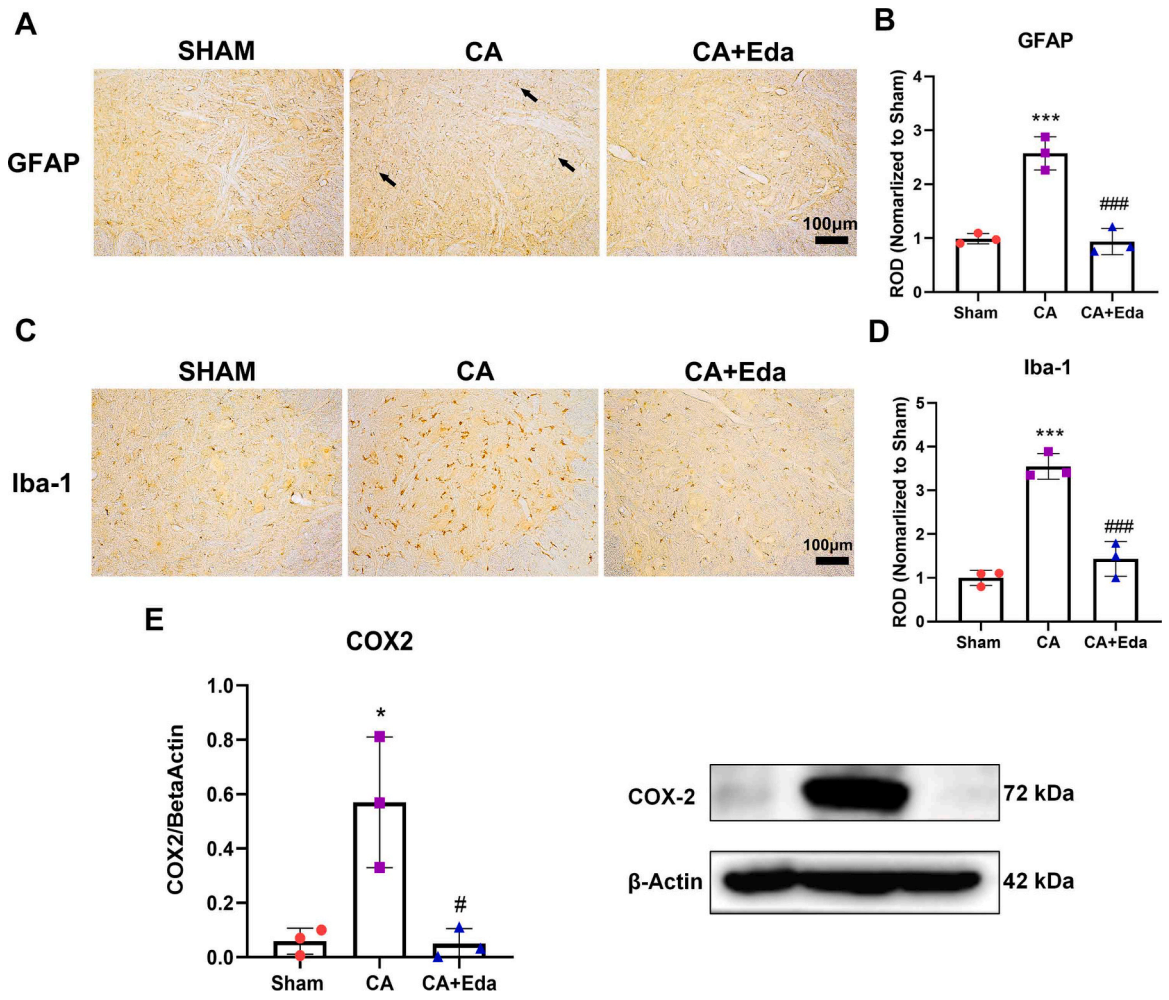

Fig. 5. Edaravone attenuates neuroinflammation in the lumbar spinal cord at 24 h after CA/ROSC (A) Representative images of GFAP immunoreactivity in the ventral horn of the lumbar spinal cord 24 h after CA/ROSC. Marked astrocytic activation with hypertrophic processes is observed in the CA group (arrows), which is attenuated in the CA + Eda group. Scale bar = 100 μm; magnification, × 200. (B) Quantification of GFAP immunoreactivity expressed as ROD normalized to the sham group. (C) Representative images of Iba−1 immunoreactivity in the ventral horn of the lumbar spinal cord 24 h after CA/ROSC. Increased microglial activation is evident in the CA group and reduced by edaravone treatment. Scale bar = 100 μm; magnification, × 200. (D) Quantification of Iba−1 immunoreactivity expressed as ROD normalized to the sham group. (E) Western blot analysis and densitometric quantification of COX−2 expression in the lumbar spinal cord. COX−2 levels were significantly increased after CA and attenuated by edaravone treatment. β-Actin was used as a loading control.Data are presented as mean ± standard deviation (SD). Statistical significance was determined using one-way ANOVA followed by Tukey's post hoc test. n = 3, respectively, * $p < 0.05$, ** $p < 0.01$, *** $p < 0.001$ vs. sham group; # < 0.05, ## $p < 0.01$, ### $p < 0.001$ vs. CA group.

therapeutic hypothermia attenuated this injury by suppressing astrocyte reactivity (Ahn et al., 2023). Delayed motor neuron degeneration accompanied by mitochondrial activation has also been observed 7 days post-asphyxial CA (Keilhoff et al., 2021), suggesting that such changes may reflect a delayed response to systemic IRI. In the present study, quantitative analysis of ChAT-positive motor neurons did not show a significant reduction in cell number at 24 h after CA/ROSC, although morphologically abnormal ChAT-positive neurons were observed. These findings support the interpretation that the 24-h time point reflects early motor neuronal injury rather than overt motor neuron loss. Nevertheless, the mechanism underlying acute-phase motor neuron injury in the lumbar spinal cord following CA remains to be elucidated. In this context, we focused on the role of ferroptosis, a regulated form of cell death that is increasingly recognized as a key contributor to central nervous system IRI (David et al., 2023). Although several studies have demonstrated the involvement of ferroptosis in brain damage after CA in porcine (Xu et al., 2021) and rat models (Min et al., 2025; Ye et al., 2023), its role in spinal cord injury has been less extensively studied.

Ferroptosis has been established as an early driver of neuronal degeneration in cerebral ischemia models (David et al., 2023), and similar involvement has been suggested in spinal cord ischemia models (Dong et al., 2023). For example, Liu et al. demonstrated that ferroptosis contributes to neurological impairment after 14 min of spinal cord ischemia, with ferrostatin−1 alleviating injury via the ERK1/2–SP1–GPX4 pathway (Liu et al., 2024). Other studies have reported that SYVN1 attenuates spinal cord IRI by inhibiting ferroptosis via the HMGB1/NRF2/HO−1 axis (Guo et al., 2023a), and that EphA4 provides protection through activation of the ERK1/2/c-Myc/transferrin receptor 1 pathway (Dong et al., 2023). To our knowledge, this study provides the first evidence that ferroptosis contributes to acute spinal motor neuron damage following CA. Within 24 h after CA, we observed mitochondrial abnormalities and changes in ferroptosis-related markers, with ACSL4 upregulation specifically localized to ChAT-positive motor neurons. These findings suggest that neuromotor deficits resulting from CA-induced spinal cord injury may be driven by ferroptosis during the acute phase. Furthermore, the marked functional improvement observed with edaravone treatment underscores the therapeutic value of early ferroptosis-targeted interventions. However, since this study did not assess iron metabolism–related markers, which are essential components of the ferroptosis

pathway (Dixon et al., 2012), further investigation is needed to fully elucidate the mechanisms involved.

Edaravone has been reported to exert anti-ferroptotic effects in models of central nervous system diseases and injuries by inhibiting lipid peroxidation via reactive oxygen species scavenging (Wang et al., 2023; Xiao et al., 2024). Edaravone has demonstrated potent anti-ferroptotic properties in various in vitro and in vivo models, including hippocampal cells and stem cell-derived motor neurons, primarily by inhibiting lipid peroxidation (Guo et al., 2023b; Martinez et al., 2023). Recent studies have highlighted the involvement of edaravone in ferroptosis regulation in central nervous system injury models. Xiao et al. reported that edaravone combined with dexborneol protects against transient middle cerebral artery occlusion-induced blood–brain barrier damage by activating the Nrf2/HO−1/GPX4 signaling pathway (Xiao et al., 2024). Pang et al. demonstrated that edaravone suppresses ferroptosis through the GPX4/ACSL4/5-LOX pathway in a traumatic spinal cord injury model (Pang et al., 2022), emphasizing that lipid metabolism-related changes, particularly in motor neurons, are critical for ferroptotic regulation.

We demonstrated that ACSL4 plays a key role in ferroptosis-mediated motor neuron damage following 5 min of cardiac arrest. Consistent with this notion, previous studies have demonstrated that ACSL4 overexpression exacerbates ischemic brain injury by promoting neuronal ferroptosis and microglia-mediated neuroinflammation (Cui et al., 2021). Western blot analysis revealed changes in both GPX4 and ACSL4 expression. Immunofluorescence revealed a selective upregulation of ACSL4 in ChAT-positive motor neurons, whereas GPX4 levels remained unchanged across all groups. This discrepancy underscores the importance of spatial and cell-type–specific analyses when interpreting ferroptosis-related proteins. Because western blotting reflects total protein expression in the whole lumbar spinal cord tissue, whereas immunofluorescence specifically evaluates ChAT-positive motor neurons in the ventral horn, tissue-level GPX4 changes may not necessarily correspond to significant alterations within motor neurons alone. Despite preserved GPX4 expression, the presence of hindlimb motor deficits and decreased GSH levels suggest that GPX4 activity may have been functionally compromised due to substrate depletion rather than being transcriptionally suppressed (Ursini and Maiorino, 2020). These findings contrast with those of Liu et al., who used a 14 min aortic arch clamping model of spinal cord IRI (Liu et al., 2024). In their study, GPX4 expression and NeuN-positive cell counts increased, whereas ACSL4 expression remained unchanged. This divergence likely stems from fundamental differences in the injury models, including the duration and extent of ischemia. CA causes whole-body ischemia followed by systemic reperfusion, initiating widespread damage and protective responses, such as the upregulation of antioxidants, anti-inflammatory cytokines, and stress-related proteins (Neumar et al., 2008). These systemic factors are unique to the cardiac arrest model and may modulate ferroptosis differently than the localized ischemia induced by aortic clamping. Thus, the expression patterns of ACSL4 and GPX4 observed in our study may reflect not only cell type specificity but also the broader pathophysiological context of cardiac arrest. Further research is needed to clarify the upstream regulators of ACSL4, including ALOX15 (Shah et al., 2018), and to investigate the downstream lipidomic changes mediated by ACSL4. Future studies should examine the functional role of GPX4 under systemic ischemic stress and clarify ferroptosis-related changes across different spinal cord cell populations to determine whether motor neurons possess intrinsic vulnerability to ACSL4-dominant ferroptosis. Complementary in vitro experiments further showed that edaravone and the ferroptosis inhibitor ferrostatin−1 attenuated H2O2-induced cytotoxicity and ACSL4 upregulation in SH-SY5Y cells, supporting the association of ACSL4-related ferroptotic signaling with oxidative neuronal injury.

In the present study, edaravone administration reduced lipid peroxidation, as evidenced by decreased MDA levels, preserved GSH levels, and GPX4 expression in the tissue, and attenuated ferroptosis-related damage in the lumbar spinal cord following CA. These effects were accompanied by the suppression of ACSL4 upregulation, particularly in spinal motor neurons. Taken together, our findings indicate that edaravone mitigates ferroptosis after cardiac arrest through multiple mechanisms, including lipid peroxidase scavenging and modulation of key ferroptosis-related proteins. Consistent with previous reports, these results extend the anti-ferroptotic profile of edaravone to a CA-induced spinal cord IRI model and support its therapeutic potential in IRI (Pang et al., 2022; Wang et al., 2023; Xiao et al., 2024).

The spinal cord contains diverse neuronal and glial populations that respond differently to ischemic injuries (Duggal and Lach, 2002). In the present study, cardiac arrest induced robust astrocyte and microglial activation in the lumbar spinal cord, as indicated by increased GFAP and Iba−1 immunoreactivity, which was attenuated by treatment with edaravone. Notably, astrocyte activation in the lumbar spinal cord has been implicated as a key pathological contributor to hindlimb paralysis following cardiac arrest in asphyxial CA models, as demonstrated by Ahn et al., where suppression of astrocytic reactivity was associated with improved motor outcomes (Ahn et al., 2023). Consistent with these observations, edaravone reduced COX−2 expression in our model, indicating the attenuation of inflammatory signaling. Although the present study focused primarily on neuronal ferroptosis, the relationship between glial activation, inflammatory signaling, and neuronal ferroptosis warrants further investigation in the context of cardiac arrest.

5. Conclusion

In conclusion, this study provides evidence that ferroptosis contributes to acute spinal motor neuron injury following cardiac arrest, characterized by the selective upregulation of ACSL4 in ChAT-positive neurons. Edaravone improved survival and motor function and attenuated ferroptosis-related damage by reducing lipid peroxidation in the lumbar spinal cord of rats. These findings support the concept that modulation of ferroptosis during the early phase after cardiac arrest may represent a potential therapeutic approach and highlight the neuroprotective potential of edaravone in spinal cord injury associated with post-cardiac arrest syndrome. Further studies are warranted to elucidate the upstream regulation of ACSL4 and the cell-type-specific functional role of GPX4 in systemic ischemia–reperfusion stress.

Funding

This research was supported by the National Research Foundation of Korea (NRF), grants funded by the Korean government (MIST) (RS−2023–00247813), Korea Institute of Planning and Evaluation for Technology in Food, Agriculture and Forestry (IPET) through Pet Industry Technology Development Program, funded by Ministry of Agriculture, Food and Rural Affairs (MAFRA) (RS−2022-IP322087) and Leading University Project for International Cooperation through the National Research Foundation of Korea(NRF) funded by the Ministry of Education(MOE) (NRF−2023H1A7A2A02000078).

CRediT authorship contribution statement

kim Ryunhee: Data curation. **Seung Hyun Lee:** Data curation. **Joonseok Lee:** Writing – original draft, Investigation, Formal analysis, Data curation, Conceptualization. **Byung-Yong Park:** Writing – review & editing, Supervision, Project administration, Funding acquisition, Conceptualization. **Su-Cheol Han:** Supervision, Project administration. **Hoang Thi Mai:** Data curation. **Hyun-Jin Tae:** Methodology. **Md Shiblee Sadik Sabuj:** Data curation.

Declaration of Competing Interest

The authors report no conflicts of interest and are solely responsible for the content and writing of this manuscript.

Appendix A. Supporting information

Supplementary data associated with this article can be found in the online version at doi:10.1016/j.brainresbull.2026.112016.

Data availability

Data will be made available on request.

References

Ahn, J.H., Lee, T.K., Kim, B., Lee, J.C., Tae, H.J., Cho, J.H., Park, Y., Shin, M.C., Ohk, T. G., Park, C.W., Cho, J.H., Hong, S., Park, J.H., Choi, S.Y., Won, M.H., 2020. Therapeutic hypothermia improves hind limb motor outcome and attenuates oxidative stress and neuronal damage in the lumbar spinal cord following cardiac arrest. Antioxidants 9, 38. https://doi.org/10.3390/antiox9010038.

Ahn, J.H., Lee, T.K., Kim, D.W., Shin, M.C., Cho, J.H., Lee, J.C., Tae, H.J., Park, J.H., Hong, S., Lee, C.H., Won, M.H., Kim, Y.H., 2023. Therapeutic hypothermia after cardiac arrest attenuates hindlimb paralysis and damage of spinal motor neurons and astrocytes through modulating Nrf2/HO-1 signaling pathway in rats. Cells 12, 414. https://doi.org/10.3390/cells12030414.

Alim, I., Caulfield, J.T., Chen, Y., Swarup, V., Geschwind, D.H., Ivanova, E., Seravalli, J., Ai, Y., Sansing, L.H., Marie, E.J.S., 2019. Selenium drives a transcriptional adaptive program to block ferroptosis and treat stroke. Cell 177, 1262–1279.e25. https://doi.org/10.1016/j.cell.2019.03.032.

Chen, Y., Fan, H., Wang, S., Tang, G., Zhai, C., Shen, L., 2021. Ferroptosis: a novel therapeutic target for ischemia–reperfusion injury. Front. Cell. Dev. Biol. 9, 688605. https://doi.org/10.3389/fcell.2021.688605.

Cheshire, W.P., Santos, C.C., Massey, E.W., Howard, J.F., 1996. Spinal cord infarction. Neurology 47, 321–330. https://doi.org/10.1212/WNL.47.2.321.

Crack, P.J., Wong, C.H., 2008. Modulation of neuro-inflammation and vascular response by oxidative stress following cerebral ischemia–reperfusion injury. Curr. Med. Chem. 15, 1–14. https://doi.org/10.2174/092986708783330585.

Cui, Y., Zhang, Y., Zhao, X., Shao, L., Liu, G., Sun, C., Xu, R., Zhang, Z., 2021. ACSL4 exacerbates ischemic stroke by promoting ferroptosis-induced brain injury and neuroinflammation. Brain Behav. Immun. 93, 312–321. https://doi.org/10.1016/j.bbi.2021.01.003.

David, S., Ryan, F., Jhelum, P., Kroner, A., 2023. Ferroptosis in neurological disease. Neuroscientist 29, 591–615. https://doi.org/10.1177/10738584221100183.

Dixon, S.J., Lemberg, K.M., Lamprecht, M.R., Skouta, R., Zaitsev, E.M., Gleason, C.E., Patel, D.N., Bauer, A.J., Cantley, A.M., Yang, W.S., Morrison, B., Stockwell, B.R., 2012. Ferroptosis: an iron-dependent form of non-apoptotic cell death. Cell 149, 1060–1072. https://doi.org/10.1016/j.cell.2012.03.042.

Doll, S., Proneth, B., Tyurina, Y.Y., Panzilius, E., Kobayashi, S., Ingold, I., Irmler, M., Beckers, J., Aichler, M., Walch, A., 2017. ACSL4 dictates ferroptosis sensitivity by shaping cellular lipid composition. Nat. Chem. Biol. 13, 91–98. https://doi.org/10.1038/nchembio.2239.

Dong, Y., Ai, C., Chen, Y., Zhang, Z., Zhang, D., Liu, S., Tong, X., Ma, H., 2023. Eph receptor A4 regulates motor neuron ferroptosis in spinal cord ischemia/reperfusion injury in rats. Neural Regen. Res. 18, 2219–2228. https://doi.org/10.4103/1673-5374.369118.

Duggal, N., Lach, B., 2002. Selective vulnerability of the lumbosacral spinal cord after cardiac arrest and hypotension. Stroke 33, 116–121. https://doi.org/10.1161/hs0102.101938.

Guo, S., Lei, Q., Guo, H., Yang, Q., Xue, Y., Chen, R., 2023b. Edaravone attenuates Aβ1–42-induced inflammatory damage and ferroptosis in HT22 cells. Neurochem. Res. 48, 570–578. https://doi.org/10.1007/s11064-022-03782-y.

Guo, L., Zhang, D., Ren, X., Liu, D., 2023a. SYVN1 attenuates ferroptosis and alleviates spinal cord ischemia–reperfusion injury in rats by regulating the HMGB1/NRF2/HO-1 axis. Int. Immunopharmacol. 123, 110802. https://doi.org/10.1016/j.intimp.2023.110802.

Ishii, H., Petrenko, A.B., Sasaki, M., Satoh, Y., Kamiya, Y., Tobita, T., Furutani, K., Matsuhashi, M., Kohno, T., Baba, H., 2018. Free radical scavenger edaravone produces robust neuroprotection in a rat model of spinal cord injury. Brain Res. 1682, 24–35. https://doi.org/10.1016/j.brainres.2017.11.014.

Kanellopoulos, G.K., Kato, H., Wu, Y., Dougenis, D., Mackey, M., Hsu, C.Y., Kouchoukos, N.T., 1997. Neuronal cell death in the ischemic spinal cord: the effect of methylprednisolone. Ann. Thorac. Surg. 64, 1279–1285. https://doi.org/10.1016/S0003-4975(97)00885-1.

Keilhoff, G., Titze, M., Rathert, H., Nguyen Thi, T.M., Ebmeyer, U., 2021. Spinal cord damage in a rat asphyxial cardiac arrest/resuscitation model. Neurocrit. Care 34, 844–855. https://doi.org/10.1007/s12028-020-01063-w.

Kubo, K., Nakao, S., Jomura, S., Sakamoto, S., Miyamoto, E., Xu, Y., Tomimoto, H., Inada, T., Shingu, K., 2009. Edaravone mitigates gray and white matter damage after global cerebral ischemia in rats. Brain Res. 1279, 139–146. https://doi.org/10.1016/j.brainres.2009.04.048.

Kudo, Y., Ohtaki, H., Dohi, K., Yin, L., Nakamachi, T., Endo, S., Yofu, S., Hiraizumi, Y., Miyaoka, H., Shioda, S., 2006. Neuronal damage in rat brain and spinal cord after cardiac arrest and massive hemorrhagic shock. Crit. Care Med. 34, 2820–2826. https://doi.org/10.1097/01.CCM.0000241157.64069.95.

Lang-Lazdunski, L., Matsushita, K., Hirt, L., Waeber, C., Vonsattel, J.P.G., Moskowitz, M. A., 2000. Spinal cord ischemia: development of a mouse model. Stroke 31, 208–213. https://doi.org/10.1161/01.STR.31.1.208.

Lee, T.K., Lee, J.C., Tae, H.J., Kim, H.I., Shin, M.C., Ahn, J.H., Park, J.H., Kim, D.W., Hong, S., Choi, S.Y., 2021. Therapeutic effects of risperidone against spinal cord injury in a rat model of asphyxial cardiac arrest. Vet. Sci. 8, 230. https://doi.org/10.3390/vetsci8100230.

Liu, S.D., Chen, F.S., Han, J., Wang, L.M., Dong, Y., 2024. Ferrostatin-1 improves neurological impairment induced by spinal cord ischemia/reperfusion injury through ERK1/2/SP1/GPX4 signaling. Exp. Neurol. 373, 114637. https://doi.org/10.1016/j.expneurol.2023.114637.

Liu, W., Wang, L., Liu, C., Dai, Z., Li, T., Tang, B., 2022. Edaravone ameliorates cerebral ischemia–reperfusion injury by downregulating ferroptosis via the Nrf2/FPN pathway. Biol. Pharm. Bull. 45, 1269–1275. https://doi.org/10.1248/bpb.b22-00363.

Martinez, A.M., Kim, A., Flores, C.A., Rahman, D.F., Yang, W.S., 2023. Mouse embryonic stem cell-derived motor neurons are susceptible to ferroptosis. FEBS Open. Bio 13, 419–433. https://doi.org/10.1002/2211-5463.13543.

Min, X.L., Shi, Y., Xu, Y., Li, Y.Y., Dong, Y.K., Chen, F.X., Chen, Q.M., Sun, Y.L., Liao, R., Wang, J.P., 2025. Mechanism of Sirtuin1-mediated deacetylation of p65-mediated ferroptosis of hippocampal neurons in cerebral injury after cardiopulmonary resuscitation in rats. Neurochem. Res. 50, 66. https://doi.org/10.1007/s11064-024-04297-4.

Neumar, R.W., Nolan, J.P., Adrie, C., Aibiki, M., Berg, R.A., Bottiger, B.W., Callaway, C., Clark, R.S.B., Geocadin, R.G., Jauch, E.C., Kern, K.B., Laurent, I., Longstreth, W.T., Merchant, R.M., Morley, P., Morrison, L.J., Nadkarni, V., Peberdy, M.A., Rivers, E.P., Rodriguez-Nunez, A., Sellke, F.W., Spaulding, C., Sunde, K., Vanden Hoek, T., 2008. Post–cardiac arrest syndrome. Circulation 118, 2452–2483. https://doi.org/10.1161/CIRCULATIONAHA.108.190652.

Özgiray, E., Serarslan, Y., Öztürk, O.H., Altaş, M., Aras, M., Söğüt, S., Yurtseven, T., Oran, İ., Zileli, M., 2012. Protective effects of edaravone on experimental spinal cord injury in rats. Pediatr. Neurosurg. 47, 254–260. https://doi.org/10.1159/000337299.

Pang, Y., Liu, X., Wang, X., Shi, X., Ma, L., Zhang, Y., Zhou, T., Zhao, C., Zhang, X., Fan, B., Hao, J., Li, W., Zhao, X., Zhang, R., Zhou, S., Kong, X., Feng, S., Yao, X., 2022. Edaravone modulates neuronal GPX4/ACSL4/5-LOX to promote recovery after spinal cord injury. Front. Cell. Dev. Biol. 10, 849854. https://doi.org/10.3389/fcell.2022.849854.

Qin, T., Lei, L.-Y., Li, N., Shi, F.R., Chen, M.-H., Xie, L., 2016. Edaravone improves survival and neurological outcomes after CPR in a ventricular fibrillation model of rats. Am. J. Emerg. Med. 34, 1944–1949. https://doi.org/10.1016/j.ajem.2016.07.009.

Rothstein, J.D., 2017. Edaravone: a new drug approved for ALS. Cell 171, 725. https://doi.org/10.1016/j.cell.2017.10.011.

Sakurai, M., Hayashi, T., Abe, K., Sadahiro, M., Tabayashi, K., 1998. Delayed and selective motor neuron death after transient spinal cord ischemia: a role of apoptosis? J. Thorac. Cardiovasc. Surg. 115, 1310–1315. https://doi.org/10.1016/S0022-5223(98)70274-1.

Shah, R., Shchepinov, M.S., Pratt, D.A., 2018. Resolving the role of lipoxygenases in the initiation and execution of ferroptosis. ACS Cent. Sci. 4, 387–396. https://doi.org/10.1021/acscentsci.7b00589.

Suzuki, K., Kazui, T., Terada, H., Umemura, K., Ikeda, Y., Bashar, A.H.M., Yamashita, K., Washiyama, N., Suzuki, T., Ohkura, K., 2005. Experimental study on the protective effects of edaravone against ischemic spinal cord injury. J. Thorac. Cardiovasc. Surg. 130, 1586–1592. https://doi.org/10.1016/j.jtcvs.2005.08.049.

Tuo, Q.-z, Liu, Y., Xiang, Z., Yan, H.-F., Zou, T., Shu, Y., Ding, X.-l, Zou, J.-j, Xu, S., Tang, F., 2022. Thrombin induces ACSL4-dependent ferroptosis during cerebral ischemia/reperfusion. Signal. Transduct. Target. Ther. 7, 59. https://doi.org/10.1038/s41392-022-00917-z.

Ursini, F., Maiorino, M., 2020. Lipid peroxidation and ferroptosis: the role of GSH and GPx4. Free. Radic. Biol. Med. 152, 175–185. https://doi.org/10.1016/j.freeradbiomed.2020.02.027.

Wang, D., Chen, F., Fang, B., Zhang, Z., Dong, Y., Tong, X., Ma, H., 2020. MiR-128-3p alleviates spinal cord ischemia/reperfusion injury associated neuroinflammation and cellular apoptosis via SP1 suppression in rat. Front. Neurosci. 14, 609613. https://doi.org/10.3389/fnins.2020.609613.

Wang, X.B., Zhou, L.Y., Chen, X.Q., Li, R., Yu, B.B., Pan, M.X., Fang, L., Li, J., Cui, X.J., Yao, M., Lu, X., 2023. Neuroprotective effect and possible mechanism of edaravone in rat models of spinal cord injury: a protocol for a systematic review and meta-analysis. Syst. Rev. 12, 177. https://doi.org/10.1186/s13643-023-02306-1.

Xiao, P., Huang, H.Y., Zhao, H.S., Liu, R.J., Sun, Z.Y., Liu, Y.S., Chen, N., Zhang, Z.L., 2024. Edaravone dexborneol protects against cerebral ischemia/reperfusion-induced blood-brain barrier damage by inhibiting ferroptosis via activation of Nrf2/HO-1/GPX4 signaling. Free. Radic. Biol. Med. 217, 116–125. https://doi.org/10.1016/j.freeradbiomed.2024.03.003.

Xu, J.F., Zhang, M.H., Liu, F., Shi, L., Jiang, X.K., Chen, C., Wang, J.A., Diao, M.Y., Khan, Z.U., Zhang, M., 2021. Mesenchymal stem cells alleviate post-resuscitation cardiac and cerebral injuries by inhibiting cell pyroptosis and ferroptosis in a swine model of cardiac arrest. Front. Pharmacol. 12, 690962. https://doi.org/10.3389/fphar.2021.690962.

Ye, Z., Zhang, F., Wang, P., Ran, Y.Q., Liu, C., Lu, J.M., Zhang, M.T., Yao, L., 2023. Baicalein relieves brain injury by inhibiting ferroptosis and endoplasmic reticulum stress in a rat model of cardiac arrest. Shock 59, 434–441. https://doi.org/10.1097/SHK.0000000000002058.

Yuan, H., Li, X., Zhang, X., Kang, R., Tang, D., 2016. Identification of ACSL4 as a biomarker and contributor of ferroptosis. Biochem. Biophys. Res. Commun. 478, 1338–1343. https://doi.org/10.1016/j.bbrc.2016.08.118.